USGS
science for a changing world

هيئة المساحة الجيولوجية السعودية
SAUDI GEOLOGICAL SURVEY

Probabilistic Seismic-Hazard Analysis for the Western Kingdom of Saudi Arabia

Chapter Q of
Active Volcanism on the Arabian Shield—Geology, Volcanology, and Geophysics of Northern Harrat Rahat and Vicinity, Kingdom of Saudi Arabia

U.S. Geological Survey Professional Paper 1862
Saudi Geological Survey Special Report SGS–SP–2021–1

U.S. Department of the Interior
U.S. Geological Survey

Cover. Photograph looking south of ground cracks cutting the basalt of Sha'ib Iskabah (152 kilo-annum [ka]). Cracks inferred to have formed during the eruption of the basalt of Southern Fingers (24 ka) located 3 kilometers north. Deposits of mafic to silicic volcanic eruptions form the skyline of the photograph, including (from left to right) scoria cones of the hawaiite of Abu Rimthah (with telecommunication towers), benmoreite of Um Junb (isolated mountain at center left), trachyte of Gura 2 (long ridge at center right), mugearite of Matan, and basalt of Al Malsaa 2. U.S. Geological Survey photograph by Andrew Calvert, November 19, 2013. Background image shows northern Harrat Rahat lava flows, maars, and lava domes. U.S. Geological Survey photograph by Andrew Calvert, January 25, 2012.

Probabilistic Seismic-Hazard Analysis for the Western Kingdom of Saudi Arabia

By Ryota Kiuchi, Walter D. Mooney, and Hani M. Zahran

Chapter Q of

Active Volcanism on the Arabian Shield—Geology, Volcanology, and Geophysics of Northern Harrat Rahat and Vicinity, Kingdom of Saudi Arabia

Edited by Thomas W. Sisson, Andrew T. Calvert, and Walter D. Mooney

U.S. Geological Survey Professional Paper 1862
Saudi Geological Survey Special Report SGS–SP–2021–1

U.S. Department of the Interior
U.S. Geological Survey

U.S. Geological Survey, Reston, Virginia: 2023

Suggested citation:
Kiuchi, R., Mooney, W.D., and Zahran, H.M., 2023, Probabilistic seismic-hazard analysis for the western Kingdom of Saudi Arabia, chap. Q *of* Sisson, T.W., Calvert, A.T., and Mooney, W.D., eds., Active volcanism on the Arabian Shield—Geology, volcanology, and geophysics of northern Harrat Rahat and vicinity, Kingdom of Saudi Arabia: U.S. Geological Survey Professional Paper 1862 [also released as Saudi Geological Survey Special Report SGS–SP–2021–1], 15 p., https://doi.org/10.3133/pp1862Q.

ISSN 1044-9612 (print)
ISSN 2330-7102 (online)

Ministry of Industry and Mineral Resources
BANDAR BIN IBRAHIM BIN ABDULLAH AL-KHORAYEF, Minister and SGS Chairman

Saudi Geological Survey
Abdullah bin Mufter Al-Shamrani, Chief Executive Officer

Saudi Geological Survey, Jiddah, Kingdom of Saudi Arabia: 2023

Contents

Figures

Conversion Factors

International System of Units to U.S. customary units

Multiply	By	To obtain
	Length	
centimeter (cm)	0.3937	inch (in.)
meter (m)	3.281	foot (ft)
kilometer (km)	0.6214	mile (mi)
meter (m)	1.094	yard (yd)
	Area	
square kilometer (km^2)	247.1	acre
square kilometer (km^2)	0.3861	square mile (mi^2)
	Volume	
cubic kilometer (km^3)	0.2399	cubic mile (mi^3)

Temperature in degrees Celsius (°C) may be converted to degrees Fahrenheit (°F) as follows:
$°F = (1.8 \times °C) + 32$.

Datum

Horizontal coordinate information is referenced to the North American Datum of 1983 (NAD 83).

Abbreviations

C.E.	Common Era
g	acceleration due to gravity
GMPE	ground-motion prediction equation
G-R	Gutenberg-Richter
ka	kilo-annum
KMZ19	GMPEs of Kiuchi and others (2019)
M	magnitude
M_L	local magnitude
M_s	surface-wave magnitude
M_w	moment magnitude
PDF	probability density function
PGA	peak ground acceleration
PGV	peak ground velocity
PSHA	probabilistic seismic hazard analysis
R_{JB}	Joyner-Boore distance
SGS	Saudi Geological Survey
SNSN	Saudi National Seismic Network
USGS	U.S. Geological Survey
V_{S30}	shear-wave velocity at 30 meters depth

Active Volcanism on the Arabian Shield
Edited by T.W. Sisson, A.T. Calvert, and W.D. Mooney
U.S. Geological Survey Professional Paper 1862
Saudi Geological Survey Special Report SGS–SP–2021–1

Chapter Q

Probabilistic Seismic-Hazard Analysis for the Western Kingdom of Saudi Arabia

By Ryota Kiuchi,[1] Walter D. Mooney,[2] and Hani M. Zahran[3]

Abstract

We present a probabilistic seismic-hazard analysis (PSHA) for the west-central part of the Arabian Peninsula. Our study area includes the northern Harrat Rahat volcanic field and the nearby city of Al Madīnah, Kingdom of Saudi Arabia. This young, active volcanic field experienced one historical eruption in 1256 C.E. (654 in the year of the Hijra) that vented 20 to 22 kilometers (km) southeast of the center of Al Madīnah, which has a present population of about 1.4 million. The field also erupted numerous times in the late Pleistocene and possibly in the early Holocene. We used recently developed regional ground-motion prediction equations for Saudi Arabia to calculate the severity of ground shaking as a function of distance from the earthquake source. This information was combined with two key volcanic parameters for this area: (1) the return period of volcanic eruptions and (2) the spatial probability of the next vent opening. The calculated ground-motion levels of peak ground acceleration and peak ground velocity with a 2-percent probability of exceedance in 50 years are expected to be about 0.14 the acceleration due to gravity (*g*) and 10 centimeters per second (cm/s), respectively, at the most probable vent opening location, about 25 km southeast of Al Madīnah's center, and about 0.07 *g* and 3 cm/s, respectively, in the city interior. These ground motions are higher than previous estimates that did not consider the nearby earthquakes associated with volcanic activity.

Introduction

Probabilistic seismic-hazard analysis (PSHA) is an important approach to ground-motion prediction for a region, and, properly done, it accounts for all possible earthquake sources. PSHA has been widely adopted as an important tool, both in seismically active regions, such as Japan, the United States, and Turkey, and in less-active regions, such as Australia and Europe, and is a key element to the creation of national seismic-hazard maps. These seismic-hazard maps guide the establishment of building codes and the estimation of potential earthquake losses related to the insurance industry.

The tectonics around the Arabian Peninsula are dominated by two processes: seafloor spreading in the Red Sea and active volcanism on the western Arabian Shield (fig. 1). Slab pull from the oceanic lithosphere beneath the Zagros Mountains (Kaban and others, 2016), removal of deep lithosphere of the Arabia Plate (Chang and others, 2011; Yao and others, 2017), and dynamic uplift by the Afar plume (fig. 1) are the forces driving the northeast movement of the Arabia Plate (Reilinger and McClusky, 2011; Kaban and others, 2016). Within the western part of the Arabian Peninsula, more than 18 continental intraplate volcanic fields, known in Arabic as "harrats," are distributed from Yemen in the south through Saudi Arabia to Turkey in the north (fig. 1; Coleman and others, 1983; Brown and others, 1989).

The most recent large earthquake swarm in the region, which included more than 30,000 earthquakes, occurred from April to June 2009 beneath the volcanic field of Harrat Lunayyir in northwestern Saudi Arabia (fig. 1*A*). The largest earthquake during this swarm was local magnitude (M_L) 5.4 according to the Saudi Geological Survey (SGS) and moment magnitude (M_w) 5.7 according to the United States Geological Survey (USGS) and was associated with a shallow magmatic dike intrusion (Pallister and others, 2010; Baer and Hamiel, 2010). In response to that earthquake and associated swarm activity, a PSHA was made for Harrat Lunayyir by Zahran and El-Hady (2017).

Harrat Rahat is one of the major volcanic fields in Saudi Arabia and is in the west-central part of the Arabian Peninsula (fig. 1). It is about 50–75 kilometers (km) wide, 310 km long, and spreads across 18,000 square kilometers (km^2) (Coleman and others, 1983; Camp and Roobol, 1989, 1991; Moufti and Németh, 2016). Harrat Rahat extends from Makkah, to the south, to Al Madīnah to the north (fig. 1). The greater Harrat Rahat area is the coalesced product of four subfields (from south to north): Harrat ar Rukhq, Harrat Turrah, Harrat Bani Abdullah, and Harrat Al Madīnah (also known

[1]Kozo Keikaku Engineering Inc.

[2]U.S. Geological Survey.

[3]Saudi Geological Survey.

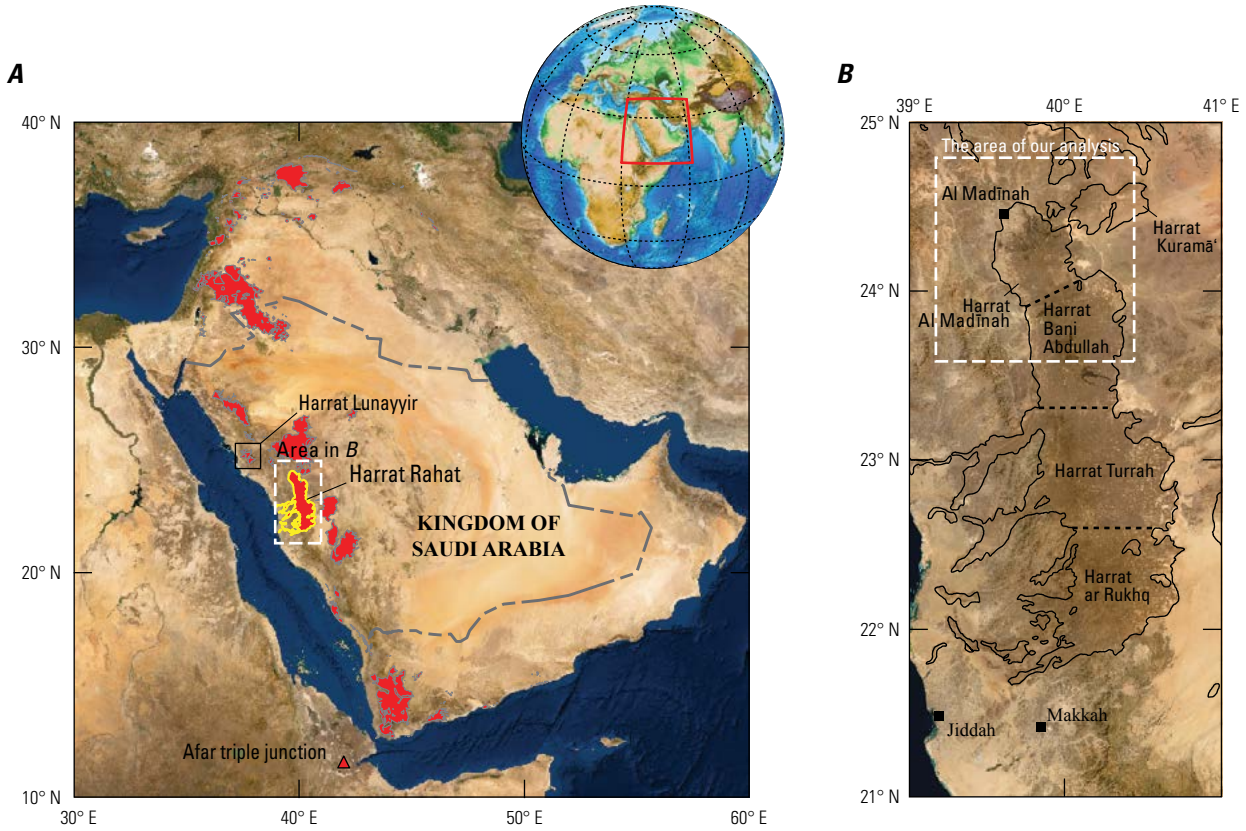

Figure 1. *A*, Satellite image of the Arabian Peninsula. Bold red square on globe shows location of the satellite image (from Esri © 2021 and its licensors). The volcanic fields on the Arabian Peninsula are shown in red. *B*, Satellite image of the Harrat Rahat volcanic field (outlined in thin black lines), along with major cities (black squares). Harrat Rahat consists of four overlapping volcanic fields. Modified from Coleman and others (1983) and Camp and Roobol (1989).

as Harrat Rashid) (fig. 1; Coleman and others, 1983, Camp and Roobol, 1989). Northern Harrat Rahat has experienced two known recent seismic episodes: (1) a seismic swarm that immediately preceded a historically recorded eruption of basaltic lava in 1256 C.E. (654 in the year of the Hijra) and (2) a 17-day-long seismic swarm in 1999 consisting of nearly 500 small (M_L 1–3) events that occurred at depths of 30 to 40 km (Lindsay and Moufti, 2014), likely owing to magmatic intrusions into the lower crust (Abdelwahed and others, 2016). Similar weak swarms may have taken place after the 1256 C.E. eruption but prior to instrumental monitoring; such weak events would have gone undetected or were unrecorded. The 1999 swarm indicates that the volcanic system in this area is still active and is a potential hazard to the city of Al Madīnah, with a population of about 1.4 million, the center of which is located 20–22 km northwest of the vents of the 1256 C.E. eruption. In addition, historical reports of the 1256 C.E. eruption indicate that it began with a strong, widely felt earthquake that was followed for several days by numerous smaller, locally felt earthquakes (Camp and others, 1987; Ambraseys and others, 2005). The volcanic activity in northern Harrat Rahat and its potential impact on the culturally significant city of Al Madīnah has motivated a number of recent geological and geophysical studies in northern Harrat Rahat (Murcia and others, 2014; Abdelwahed and others, 2016; Yao and others, 2017; Dietterich and others, 2018, 2023; Downs and others, 2018, 2019, 2023; Stelten and others, 2018, 2020, 2023; Bedrosian and others, 2019; Civilini and others, 2019; Langenheim and others, 2019, 2023; Peacock and others, 2023).

In the 2007 version of the Saudi Building Code (SBC-301-2007) (Saudi Building Code National Committee, 2007) and the recent seismic hazard map published by Zahran and others (2015, 2016), the area of northern Harrat Rahat is not included as one of the seismic zones. Here we present an assessment of the strength of ground shaking that can be expected for earthquakes that might occur near Al Madīnah. Few earthquakes have been recorded in northern Harrat Rahat since the Saudi National Seismic Network (SNSN) was installed in 2004 (some seismometers were installed and operational prior to the SNSN). Therefore, to perform this PSHA we adopted two assumptions based on volcanic studies in this area. The first assumption is that the recurrence period of volcanic eruptions derived by Stelten and others (2023) can

be used as the recurrence interval of earthquakes. The second assumption is that the spatial probability model of the next vent opening in northern Harrat Rahat (Dietterich and others, 2017) can be used as the areal source model in the PSHA. Hence, we base this probabilistic seismic-hazard model on the assumption that any future strong earthquakes will accompany significant volcanic activity. To the best of our knowledge, this PSHA is the first seismic hazard model based on both seismic and volcanic research results. In the absence of a good record of past earthquakes, this analysis uses the association of earthquakes with magmatic activity to provide an estimate of the seismic hazard for the populated areas around Harrat Rahat.

Methodology

Workflow of this PSHA

In terms of seismic hazard analysis, to estimate the possible ground motions caused by a single scenario earthquake, a deterministic seismic-hazard analysis would be an appropriate method. However, PSHA accounts for the potential effect of ground motions from multiple events. Our PSHA considered a series of earthquakes that would accompany volcanic activity. PSHA is the evaluation of the frequency of the exceedance of specific ground motion levels at a site (McGuire, 2008), and the analysis may be divided into five steps: (1) identify earthquakes that may produce the damaging ground motions at sites of interest; (2) obtain the annual rate at which earthquakes at various magnitudes are expected to occur; (3) characterize the distribution of source-to-site distances associated with potential earthquakes; (4) predict the mean and uncertainties of ground motion using ground motion prediction equations (GMPEs); and (5) combine the results obtained in steps 1–4 to calculate a full probabilistic distribution of levels of ground motion and their associated rates of exceedance (Baker and others, 2021). As mentioned above, we focused on earthquakes accompanying volcanic activity in the area of Al Madīnah located in the northern end of Harrat Rahat and only considered these earthquakes in step 1. For step 2, we used the recurrence interval of volcanic eruptions in northern Harrat Rahat based on the detailed geochronology results presented by Stelten and others (2023). The spatial probability distribution of future volcanic eruptions in northern Harrat Rahat are presented by Dietterich and others (2017) and were used in step 3. We adopted the GMPEs presented by Kiuchi and others (2019), which are important to predictions of ground motion from a given earthquake in step 4. Steps 2, 3, and 4 are described in detail below.

Historic Eruptions and Recurrence Intervals

PSHA requires knowing the recurrence interval of earthquakes. Here, we assumed that events that may cause ground motions in Al Madīnah will, as in the past, accompany volcanic eruptions close to the city. To estimate the frequency of volcanic eruptions of Harrat Rahat, Stelten and others (2023) employed $^{40}Ar/^{39}Ar$ and ^{36}Cl surface-exposure geochronologic dating to measure the ages of lava flows, lava domes, and pyroclastic deposits identified by geologic maps in northern Harrat Rahat. In total, they determined 168 $^{40}Ar/^{39}Ar$ and 10 ^{36}Cl ages in their study. Their results show that the recurrence intervals between the past volcanic eruptions range from hundreds of years to approximately 15,000 years. They assumed that the volcanic eruptions in Harrat Rahat follow a Poisson distribution to estimate a statistically reliable average recurrence interval of eruptions. Note that the estimated recurrence interval from the Poisson distribution is independent of how many years have passed since the last eruptions. The probability of eruption within a given number of years can then be estimated from the average recurrence interval. The analysis of the recurrence interval is based on the last 180,000 years, for which the volcanic record is considered to be largely complete. The data used for this analysis consist of the samples directly dated by $^{40}Ar/^{39}Ar$ and ^{36}Cl methods, as well as other volcanic deposits whose ages were bracketed by dating overlying and underlying rocks and by other geologic and paleomagnetic evidence (totaling 102 known or estimated ages; Stelten and others, 2023). As a result, the average recurrence interval obtained by fitting the Poisson probability density function is 3,200 years. The single Poisson model, however, fails to match the short-duration intervals between eruptions of northern Harrat Rahat, whereas a mixed exponential (or mixed Poisson) process provides a closer description. This mixed exponential process consists of a long repose state, averaging 4,000 years, and a short repose state, averaging 220 years (Stelten and others, 2023). Estimating uncertainties for these averages is hindered by their descriptive, rather than mechanistic, determinations, but applying a conservative 20-percent relative uncertainty to each average repose and considering that 766 years have passed since the 1256 C.E. eruption (as of 2022 C.E.), yields present-day eruption probabilities for northern Harrat Rahat of 0.029±0.008 percent annually, 1.4±0.4 percent in the next half century, and 23±4 percent in the next millennium (Stelten and others, 2023).

The SNSN shows that shallow, moderate (M_w 5.7) earthquakes, similar to events at Harrat Lunayyir in 2009, may occur owing to the emplacement of dikes within several kilometers of the ground surface. Such events can produce significant, damaging ground shaking without an accompanying eruption. Open ground cracks mapped in northern Harrat Rahat show that such “failed eruptions” occurred in this field in the past. Three sets of gaping ground cracks were mapped in northern Harrat Rahat. Two sets of ground cracks cut lava flows dated at 149±10 kilo-annum (ka) and 217±8 ka, and the third cuts a flow bracketed between 50±9 ka and 129±8 ka. Rock exposures are excellent in the field area, but these ground cracks are subtle and, conservatively, an equal number of such cracks might be obscured. Six “failed eruptions” in the area over

the past 217,000 years, sufficiently large to produce ground cracking, is, however, a number relatively small compared to documented eruptions over the time span and would not change estimates of seismic frequency.

In many large volcanic fields around the world, magnitude (*M*) 7 or larger earthquakes have occasionally accompanied volcanic eruptions, including earthquakes in Kīlauea, Hawai‘i (the 1868 *M*7.9 event, the 1975 surface-wave magnitude [M_s] 7.2 event, and the 2018 M_w 6.9 event), and the 1914 *M*7 event in Sakurajima (Yokoyama, 1986; Eissler and Kanamori, 1987; Klein and Wright, 2008; Kehoe and others, 2019). Each of these earthquakes is in a unique tectonic setting, making direct comparisons questionable, and large earthquakes are quite rare in comparison with the number of volcanic eruptions that have occurred worldwide. The eruptive flux of northern Harrat Rahat (~0.1 cubic kilometers per thousand years [km^3/k.y.]) (Stelten and others, 2020, 2023) is several orders of magnitude smaller than the volcanic areas at Kīlauea, Hawai‘i (100–200 km^3/k.y.) (Lipman and Calvert, 2013), and Sakurajima, Japan (~1 km^3/k.y.) (Aizawa and others, 2011). Consequently, it is reasonable to assume that the largest expected earthquake will be smaller than *M*7 based on the overall size of the volcanic system in northern Harrat Rahat. The PSHA hazards maps for Harrat Lunayyir of Zahran and El-Hady (2017) assumed maximum earthquake sizes of M_w 6–6.4 on the basis of the largest earthquake (M_w 5.7) during the 2009 Harrat Lunayyir seismic swarm. In our analysis, we assume that the largest earthquake to occur will have a maximum local magnitude of M_L 6.5.

The expected seismicity related to northern Harrat Rahat can also be estimated by the Gutenberg-Richter (G-R) magnitude-frequency law (Gutenberg and Richter, 1944):

$$\log_{10}\lambda_m = a - bm, \tag{1}$$

where

λ_m is the number or rate of earthquakes larger than magnitude *m*, and

a and *b* are constants derived on the basis of observation and the historical earthquake catalog.

In practice, the upper and lower earthquake-magnitude bounds have to be assumed when using the G-R law in PSHA to avoid calculations for small, unfelt earthquakes or unreasonably large earthquakes. As discussed above, we hypothesized M_L 6.5 as the upper bound for the earthquake magnitude in our analysis. Most PSHA studies use a lower bound of magnitude M_L 4.5 to 5, because earthquakes smaller than this bound have such short duration that they do not cause damage even if they generate high peak ground acceleration (PGA). In our PSHA we assume the lower bound of the magnitude to be M_L 3, and we note that this can slightly increase the ground motions estimated for a specific probability as compared to using a lower bound of M_L 4.5 to 5. However, this increase is likely small compared to other uncertainties in our model. A cumulative density function for the magnitudes of earthquakes between lower and upper bound magnitudes can be derived based on equation 1 (Baker and others, 2021):

$$\begin{aligned} F_M(m) &= P(M \le m | m_{\min} < M < m_{\max}) \\ &= \frac{\text{Rate of earthquakes with } m_{\min} < M \le m}{\text{Rate of earthquakes with } m_{\min} < M \le m_{\max}} \\ &= \frac{\lambda_{m_{\min}} - \lambda_m}{\lambda_{m_{\min}} - \lambda_{m_{\max}}} \\ &= \frac{10^{a-bm_{min}} - 10^{a-bm}}{10^{a-bm_{min}} - 10^{a-bm_{max}}} \\ &= \frac{1-10^{-b(m-m_{\min})}}{1-10^{-b(m-m_{\max})}}, \qquad (m_{\min} < m < m_{\max}), \end{aligned} \tag{2}$$

where

$F_M(m)$ is the cumulative density function for magnitudes;

$m_{\min}$ and $m_{\max}$ are lower (M_L 3) and upper (M_L 6.5) bounds, respectively, of magnitude in our analysis; and

$P(M \le m | m_{\min} < M < m_{\max})$ is the probability of an event with magnitude (M) $\le m$ in the interval between $m_{\min}$ and $m_{\max}$.

Equation 2 can be converted to a probability density function for magnitudes

$$\begin{aligned} f_M(m) &= \frac{d}{dm} F_M(m) \\ &= \frac{d}{dm}\left(\frac{1-10^{-b(m-m_{\min})}}{1-10^{-b(m-m_{\max})}}\right) \\ &= \frac{b\ln(10)10^{-b(m-m_{\min})}}{1-10^{-b(m_{\max}-m_{\min})}}, \qquad (m_{\min} < m < m_{\max}). \end{aligned} \tag{3}$$

Equations 2 and 3 are continuous distributions of magnitudes. A discrete probability distribution can be calculated based on the cumulative density function in equation 2:

$$P(M = m_j) = F_M(m_j + 1) - F_M(m_j), \tag{4}$$

where

m_j are the discrete set of magnitudes in the range of $m_j < M < m_{j+1}$.

The discrete magnitude bin must be small to obtain robust results in PSHA, so we adopt M_L 0.1 as the magnitude bin, which is a typical value in a practical PSHA.

Because we fix the recurrence interval of an M_L 6.5 event based on the return period of volcanic eruptions, the *b*-value of the G-R law is the key parameter to describe how often smaller events occur compared to our upper bound of M_L 6.5. There is no event catalog that includes enough earthquakes to calibrate the *b*-value in the G-R law, so we assumed a *b*-value of 0.895 as derived by Zahran and El-Hady (2017) for Harrat Lunayyir from the local earthquake catalog (fig. 2). Furthermore, we truncated the G-R law at an assumed maximum magnitude of M_L 6.5. The location of this background seismicity is also hypothesized to follow the spatial probability distribution of the vent opening, similar to the largest event.

As stated above, we hypothesized that the recurrence period of volcanic eruptions is equivalent to the recurrence of a M_L 6.5 event. Combining this hypothesis with the truncated G-R law and $b = 0.895$ indicates an earthquake rate of about 7.85 times for M_L 5.5 and about 2.8 times for M_L 6. Also, with this hypothesis one event with M_L 6.5 occurs with a strong volcanic eruption in northern Harrat Rahat (fig. 2). Since many volcanic eruptions are not accompanied by earthquakes reaching M_L 6.5, this assumption overestimates seismic hazards, but the volcano-seismic record in Saudi Arabia is insufficient for more refined estimates.

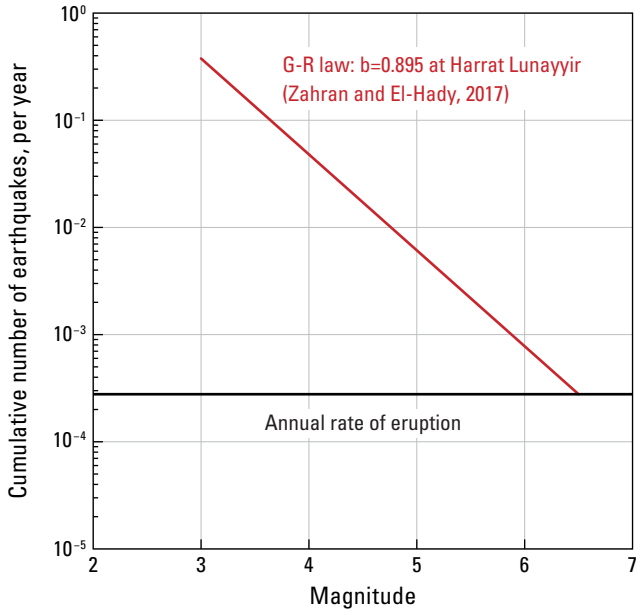

Figure 2. Plot of cumulative earthquakes per year versus magnitude. Red line shows Gutenberg-Richter (G-R) magnitude-frequency law used in this study; black line shows annual rate of volcanic eruption in northern Harrat Rahat, derived by Stelten and others (2023).

Spatial Probability Distribution for Future Eruptions

In step 3, earthquakes accompanying volcanic activity are assumed to occur at the sites of basaltic volcanic eruptions. Accordingly, we used the spatial probability distribution of the next vent opening calculated by Dietterich and others (2017) as the distribution for the earthquake locations. In general, volcanic eruptions tend to occur around areas with clusters of young volcanic vents. Northern Harrat Rahat's greatest cluster of young vents spans from about 20 to 35 km south-southeast from Al Madīnah's center with vents aligned in the north-northwest–south-southeast direction. Based on the distribution of previously erupted vent centroids and their ages, Dietterich and others (2017) estimated the spatial probability of the next basaltic vent opening across this area using an anisotropic kernel density method, similar to the approach presented by El Difrawy and others (2013). We modified the approach of El Difrawy and others (2013) by assigning greater weights to younger vents compared to older ones. The results indicate that the highest probability area of vent opening (fig. 3) is near the northern end of the vent cluster and is spread out in a north-south direction. The most probable site for the next eruption is located about 25 km south from the center of the city of Al Madīnah.

Ground Motion Prediction Equations Used for PSHA

The GMPEs for western Saudi Arabia were developed by Kiuchi and others (2019) and are referred to as KMZ19. These regional GMPEs are based on the GMPEs of Boore and others (2014) (referred to as BSSA14) as a reference model but were modified using regional earthquakes, including the 2009 Harrat Lunayyir seismic swarm. The BSSA14 model is based on the Next Generation Attenuation-West2 (NGA-West2) project GMPEs (Bozorgnia and others, 2014) that were developed for shallow crustal earthquakes using a global dataset. The KMZ19 model has the same functional form as the BSSA14 model that was derived from a large dataset covering a wide range of distances and earthquake magnitudes. The smaller dataset used in KMZ19 consists of 2,761 seismograms recorded at 77 stations from 225 events with magnitudes M_L 3 to 5.4 and assumes an equivalence of local magnitudes and moment magnitudes as discussed by Kiuchi and others (2019). About 80 percent of the events in the KMZ19 dataset occurred during the 2009 Harrat Lunayyir swarm, which was driven by a magmatic dike intrusion (Pallister and others, 2010). The main modification to the reference model is the smaller magnitude scaling for PGA in KMZ19 compared to the BSSA14 model. In contrast, the KMZ19 model has a lower anelastic attenuation (higher Q-value), which is expressed in terms of the distance scaling in the KMZ19 GMPEs compared to the BSSA14 model. Since the KMZ19 model was developed using earthquakes within the magnitude range of M_L 3–5.4,

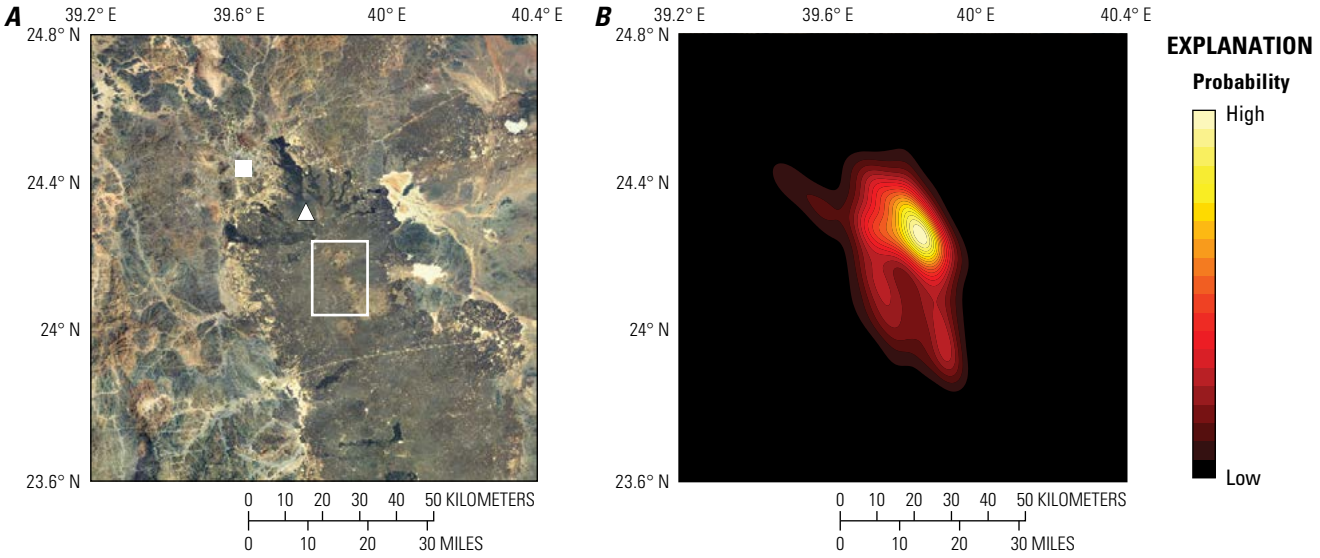

Figure 3. Maps of northern Harrat Rahat volcanic area. *A*, Satellite image (from Esri © 2021 and its licensors). *B*, Equal map area showing the spatial probability of vent opening for the next basaltic eruption in northern Harrat Rahat (Dietterich and others, 2017). White square shows center of Al Madīnah, white triangle shows vent location of the 1256 C.E. eruption, and white outlined rectangle shows location of the 1999 seismic swarm. Al Madīnah is 20 km from the vent location of the 1256 C.E. eruption.

we needed to extrapolate the ground motion values for the larger earthquakes (M_L 5.5 to 6.5) in this hazard study. We followed the KMZ19 assumption that extrapolating to a larger magnitude range follows the same trends of the magnitude scaling as for the BSSA14 model (Kiuchi and others, 2019).

In computing GMPEs for this area we also needed to include local site effects. The volcanic thickness in the study area was estimated based on the gravity survey of Langenheim and others (2019, 2023). The average estimated thickness of low-density volcanic rocks and possible underlying sediments is about 200 meters (m), and this generally matches the constructional relief of the volcanic field, consistent with most of the low-density material being volcanic with no appreciable thicknesses of underlying sediments atop the Proterozoic basement. Low density materials reach their greatest thicknesses of about 600 m where constructional relief of the volcanic field approaches its greatest height southeast of the 1256 C.E. eruption vent; this thickness exceeds constructional volcanic relief and indicates a shallow basin, probably a graben, beneath the volcanic axis (Langenheim and others, 2023). The volcanic thickness around the city of Al Madīnah is quite thin at less than 100 m. The site amplification around Al Madīnah is expected to be small whereas the ground motion might be amplified around the location of the 1256 C.E. eruption. Therefore we assumed a shear-wave velocity at 30 m depth (V_{S30}) of 760 meters per second (m/s), corresponding to a firm rock site in our analysis.

In the PSHA framework, GMPEs are used to quantify the probability of ground motion for a given earthquake as a function of earthquake magnitude and source-to-site distance. Because GMPEs consist of a predicted mean and the associated standard deviation, the probability of exceeding ground motion level a for a given magnitude m and distance r can be described as follows (Baker and others, 2021):

$$P\left(IM > a|m,r\right) = 1 - \Phi\left(\frac{\ln a - \overline{\ln IM\left(m,r,V_{S30}\right)}}{\sigma\left(m,r\right)}\right), \quad \text{and} \quad (5)$$

$$\sigma\left(m,r\right) = \sqrt{\tau^2\left(m\right) + \phi^2\left(m,r\right)},$$

where

Φ is the standard normal cumulative distribution function;

IM is the ground motion intensity measure such as PGA or peak ground velocity (PGV);

$\overline{\ln IM}$ is the mean value predicted by GMPEs; and

σ is the total standard deviation of 1n IM, which is divided into the between-event and within-event standard deviations (τ and ϕ, respectively).

Combining Recurrence Period, Spatial Probability, and GMPEs

Combining all the results derived in steps 1 through 4, we compute the probability of exceeding a ground-motion level, a, of a future earthquake for a single source at a given site as follows (Baker and others, 2021):

$$P\left(IM > a\right) = \int_{m_{\min}}^{m_{\max}} \int_{0}^{r_{\max}} P\left(IM > a|m,r\right) f_M\left(m\right) f_R\left(r\right) dr\, dm, \quad (6)$$

where

$P(IM > a|m, r)$ is obtained in step 4 (eq. 5) using GMPEs;

$f_M(m)$ is the probability density function (PDF) for magnitudes m, as described in equation 3; and

$f_R(r)$ is the PDF for distances of r.

Variability in ground motions, also known as aleatory sigma, is included in the calculation of P (probability) in equation 6. In our analysis, we used the spatial probability distribution of earthquake source locations (fig. 3) derived from Dietterich and others (2017) instead of the simple areal source locations in which the probability is homogeneously distributed. Therefore, we can rewrite equation 6 as follows:

$$P(IM > a) = \int_{m_{\min}}^{m_{\max}} \int_{x_{\min}}^{x_{\max}} \int_{y_{\min}}^{y_{\max}} P(IM > a|m,r) f_M(m) f_{\text{Source}}(x,y)\, dx\, dy\, dm, \quad (7)$$

where

$f_{\text{Source}}(x,y)$ is the spatial probability distribution of earthquake source locations as shown in figure 3;

x and y correspond to longitude and latitude, respectively; and

r is the Joyner-Boore distance (R_{JB}), which is the closest distance from a site to the surface projection of an earthquake rupture plane.

These factors are then integrated over all magnitudes and distances under consideration. In addition, we incorporate the rate of occurrence of earthquakes derived in step 2 into the probability calculation in equation 7:

$$\lambda(IM > a) \quad (8)$$

$$= \lambda(IM > \mathrm{m}_{\min})\, P(IM > a)$$

$$= \lambda(M > m_{\min}) \int_{m_{\min}}^{m_{\max}} \int_{x_{\min}}^{x_{\max}} \int_{y_{\min}}^{y_{\max}} P(IM > a|m,r) f_M(m) f_{\text{Source}}(x,y)\, dx\, dy\, dm,$$

where

$\lambda(M > m_{\min})$ is the rate of occurrence of earthquakes larger than $m_{\min}$ from the assumed source locations.

In practice, the calculation for equation 8 can be then rewritten as a discrete summation:

$$\lambda(IM > a) = \quad (9)$$

$$\lambda(M > m_{\min}) \sum_{j=1}^{n_M} \sum_{k=1}^{n_x} \sum_{l=1}^{n_y} P(IM > a|m_j, r_{kl})\, P(M = m_j)\, P(X = x_k, Y = y_l),$$

where

n_M, n_x, and n_y are the numbers of intervals for the range of M, x, and y, respectively.

In most seismic hazard maps, such as the 2014 U.S. National Seismic Hazard Model (Petersen and others, 2015), the estimates of possible ground shaking at the sites of interest are provided as the probability of exceeding a given level of ground motion within a specified time interval. This calculation is achieved by assuming that the probability distribution of time between earthquakes follows a Poisson distribution, which is time-independent for the occurrence of earthquakes. Here we consider earthquakes that are the products of future volcanic eruptions in the northern Harrat Rahat volcanic field. The combination of eruptions that follow a Poisson process with multiple earthquakes resulting from each eruption results in a highly clustered distribution of earthquakes (Llenos and Michael, 2022). However, we can assume a Poisson process if we only estimate the probability of a single exceedance and limit our results to small probabilities of exceedance, such as 10 percent or less in 50 years (Marzocchi and Taroni, 2014). This is convenient because the mathematical equations can be simplified. Under this assumption, the probability of observing exceedance of a given ground motion level, a, in a period of time, t, is as follows:

$$P(IM > a,t) = 1 - e^{-\lambda(IM > a)t}, \quad (10)$$

where

λ is the rate of occurrence obtained in equation 9.

From equation 10, we estimated probabilities for any given ground-motion levels. Conversely, for a given probability we can estimate ground-motion levels.

Results

We carried out PSHA using recurrence intervals, spatial probability distribution of the next vent opening, and GMPEs. From equation 9, we estimated probabilities for a given level of ground motion, and we can also calculate ground-motion levels for a given probability. In the colored plots of figures 4 and 5, instead of plotting the probability determined by equation 8, we plotted the level of ground motion for a specific probability, which can also be calculated using equation 8. This is the conventional way of plotting probabilistic ground-motion results. The expected ground-motion distributions in the case of a 2-percent probability of exceedance in 50 years are shown for both PGA and PGV (fig. 4). The spatial distribution of both PGA and PGV are quite similar but the decay with distance from the highest value is greater for PGV. The largest PGA and PGV values are distributed at the most probable vent opening location where there is the greatest concentration of young volcanic vents. For that area, the largest values of PGA and PGV are about 0.16 acceleration due to gravity (g) and 7 centimeters per second (cm/s), respectively. The values of PGA and PGV decrease away from the locus of the youngest vents but are as large as about 0.07 g and 3 cm/s at the center of Al Madīnah. The hazard curves corresponding to these two locations are shown for PGA and PGV (fig. 5). The highest values of PGA and PGV for all time periods correlate with the most probable vent opening location, whereas lower PGA and PGV values are estimated at the center of Al Madīnah (fig. 5). The trends of the hazard curves of these two locations are quite similar.

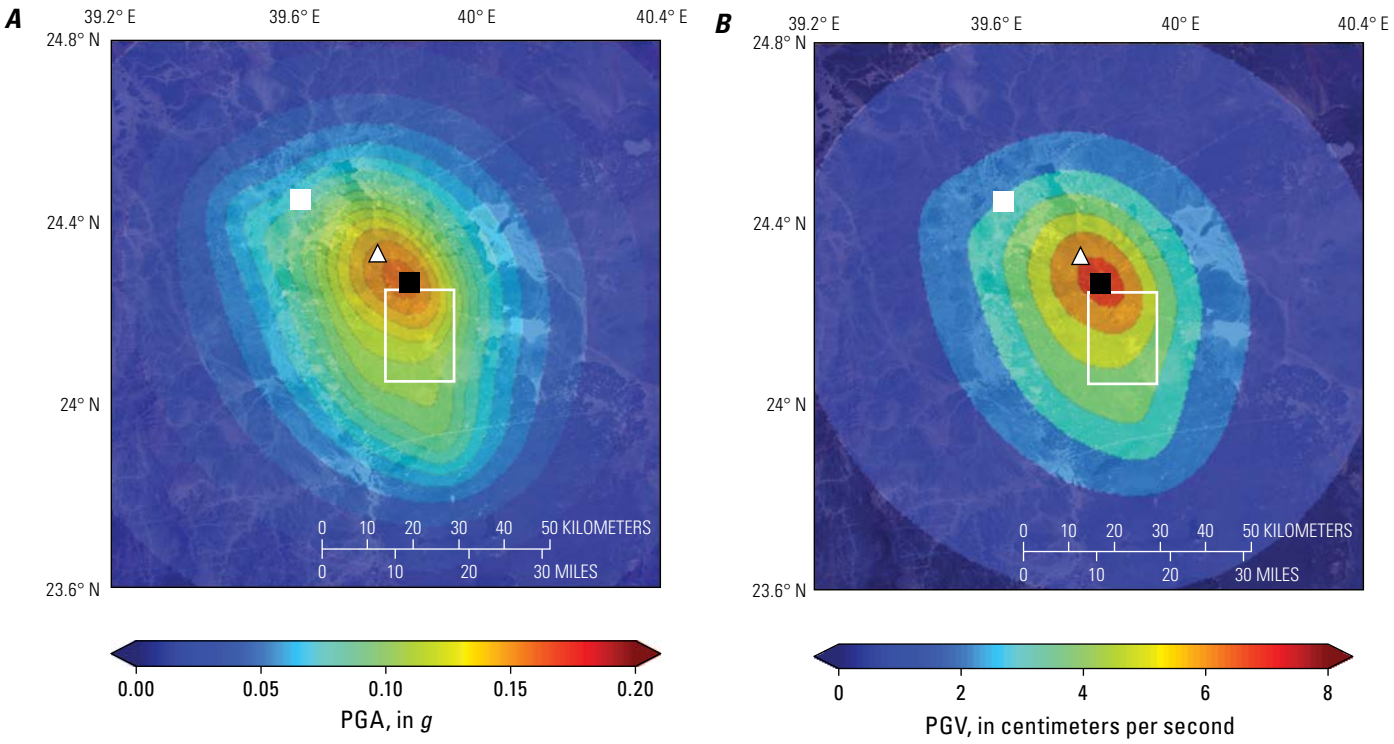

Figure 4. Maps of the expected peak ground acceleration (PGA) (*A*) and peak ground velocity (PGV) (*B*) for a 2-percent probability of exceedance in 50 years (2,475-year return period) using the spatial distribution of Dietterich and others (2017). White square shows center of Al Madīnah, white triangle shows vent location of the 1256 C.E. eruption; black square shows location of the most probable vent opening, and white outlined rectangle shows location of the 1999 earthquake swarm. *g*, acceleration due to gravity.

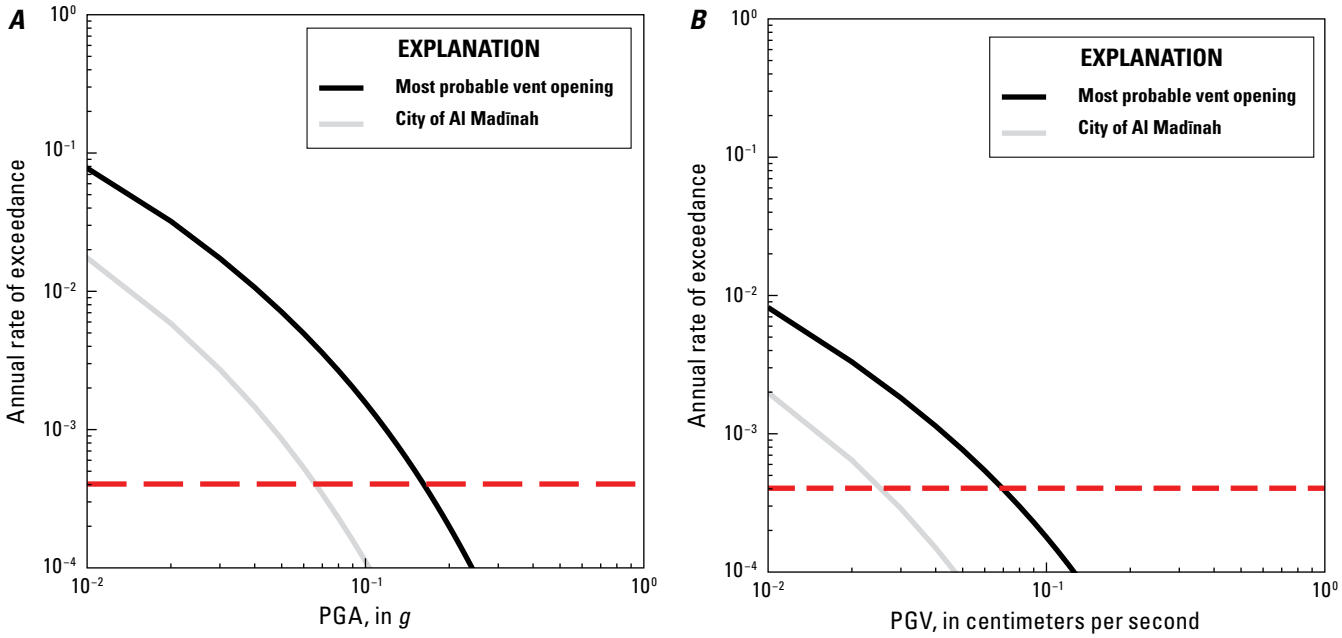

Figure 5. Plots showing hazard curves of peak ground acceleration (PGA) (*A*) and peak ground velocity (PGV) (*B*) for the location of the most probable vent opening (black line) and for the center of Al Madīnah (gray line), as shown in figure 4. Red dashed line is the annual rate of exceedance of 0.000404 (2,475-year return period). *g*, acceleration due to gravity.

Deaggregation

We performed a deaggregation analysis to identify the magnitudes and source locations of earthquakes that contribute to our seismic-hazard analysis at a specific ground-motion level for a site of interest. Since PSHA is integrated over the range of all magnitudes and source locations, the process of deaggregation is used to determine the relative contribution of each earthquake source zone to the total seismic hazard.

To perform deaggregation, we first need to calculate the rate of occurrence as obtained in equation 9 but without integrating over either magnitude or distance (Baker and others, 2021):

$$\lambda\left(IM > a, M = m, R = r\right) = \lambda\left(M > m_{\min}\right) P\left(IM > a | m, r\right) P\left(M = m\right) P\left(R = r\right). \quad (11)$$

We then derive the conditional distribution of magnitudes and distances by dividing equation 11 by equation 9:

$$P\left(M = m, R = r \middle| IM \rangle a\right) = \frac{\lambda\left(IM > a, M = m, R = r\right)}{\lambda\left(IM > a\right)}. \quad (12)$$

Discretization for magnitudes and distances is needed to apply equation 12 to our results. We adopt discretized intervals as follows: (1) 0.25 units for magnitude and (2) 5 km for distance. Figure 6 shows the results of deaggregation at the center of Al Madīnah for the case of a PGA value of 0.07 *g* and a PGV value of 3 cm/s (fig. 3*B*). These results correspond to a 2-percent probability of exceedance in 50 years (2,475-year return period) as shown in figure 4. The result of deaggregation for PGA reveals that the largest contributions to the total seismic hazard are the source magnitude (here M_L 5.25–5.5) and the distance (10–15 km) as shown in figure 6*A*. At greater distances, the contribution of these factors is reduced, especially for lower magnitudes. For PGV, M_L 5.75–6.25 sources 10 to 20 km away from the center of Al

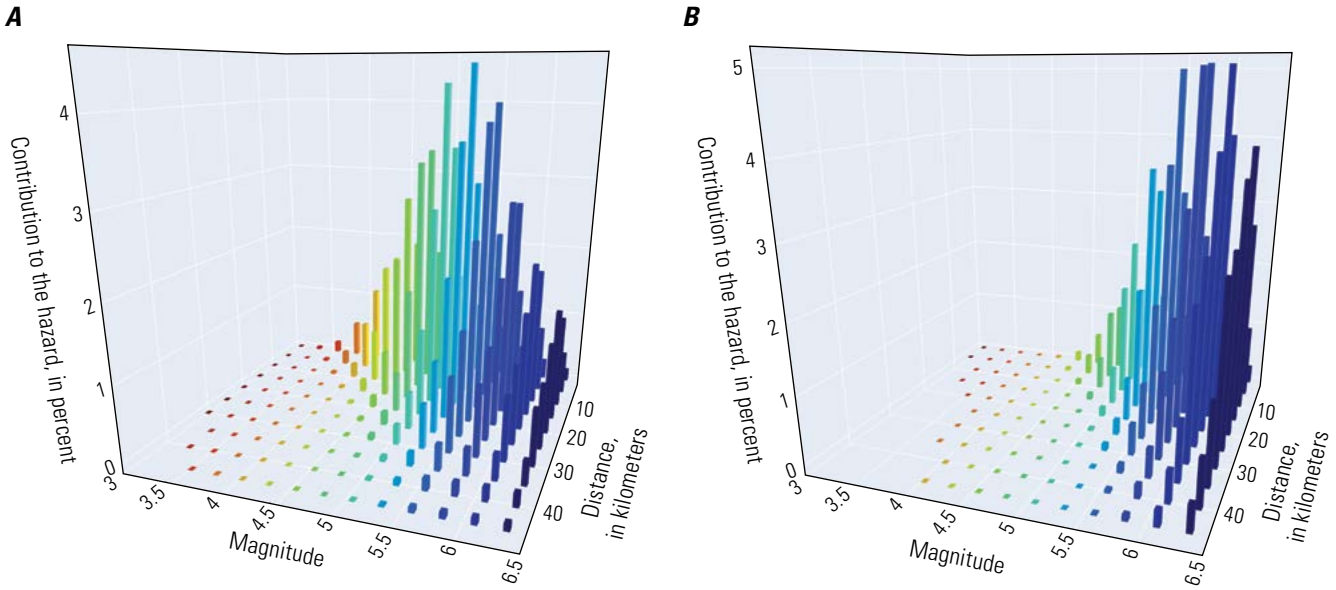

Figure 6. Three-dimensional bar plots of deaggregation results in terms of epicentral distances from the center of Al Madīnah and magnitudes for both peak ground acceleration (PGA) (*A*) and peak ground velocity (PGV) (*B*). The deaggregation results indicate values of 0.07 standard gravity (*g*) for PGA and 3 centimeters per second for PGV, which are estimated as a 2-percent probability of exceedance in 50 years (2,475-year return period) using the spatial distribution of Dietterich and others (2017) displayed in figure 3*B*. Colors are keyed to magnitudes in the bar plots.

Madīnah are the primary contribution to the total seismic hazard (fig. 6*B*). The differences in the relative contributions to the seismic hazard for PGA and PGV are due to the different magnitude and distance scaling of GMPEs for PGA versus PGV. Note that the largest contributed source for both locations (fig. 6) is not the single largest event (M_L 6.5) accompanied by the volcanic eruption. The reason is that the recurrence interval of volcanic eruption, about 4,000 years, is longer than the 2,475-year return period (2-percent probability of exceedance in 50 years). The location of the most probable vent opening corresponds to magnitudes between *M*5 and 5.5 for PGA and *M*5.75 and 6.25 for PGV (fig. 4).

Looking more closely at which source contributes the most to the seismic hazard, we estimate the conditional distribution of magnitudes and source locations as derived in equation 12:

$$\lambda\left(IM > a, M = m, X = x, Y = y\right) = \tag{13}$$

$$\lambda\left(M > m_{\min}\right) P\left(IM > a | m, r\right) P\left(M_i = m\right) P\left(X = x, Y = y\right), \text{ and}$$

$$P\left(M = m, X = x, Y = y \middle| IM > a\right) = \frac{\lambda\left(IM > a, M = m, X = x, Y = y\right)}{\lambda\left(IM > a\right)}.$$

Figure 6 shows the results of deaggregation using equation 13 for the center of Al Madīnah and the location of the most probable vent opening. The source location that contributes the most to both PGA and PGV in the center of Al Madīnah is located several kilometers southeast of the city center where the source probability is small (fig. 3*B*). The area that contributes higher magnitude sources (~M_L 6) is further from the city center than the area with M_L 5 sources (fig. 7).

From the results of the deaggregation analysis, we find that the seismic hazard in Al Madīnah is mainly affected by sources closest to the city with *M*5.25–5.75 for PGA and *M*5.5–6 for PGV. Although areas within 5 km of the city have to be carefully considered, the probability of occurrence of an earthquake close to the city is small for three reasons: (1) there is a low probability of vent opening close to the city (Dietterich and others, 2017); (2) the recent seismic swarm in 1999 occurred south of the location of the 1256 C.E. eruption, not near the city

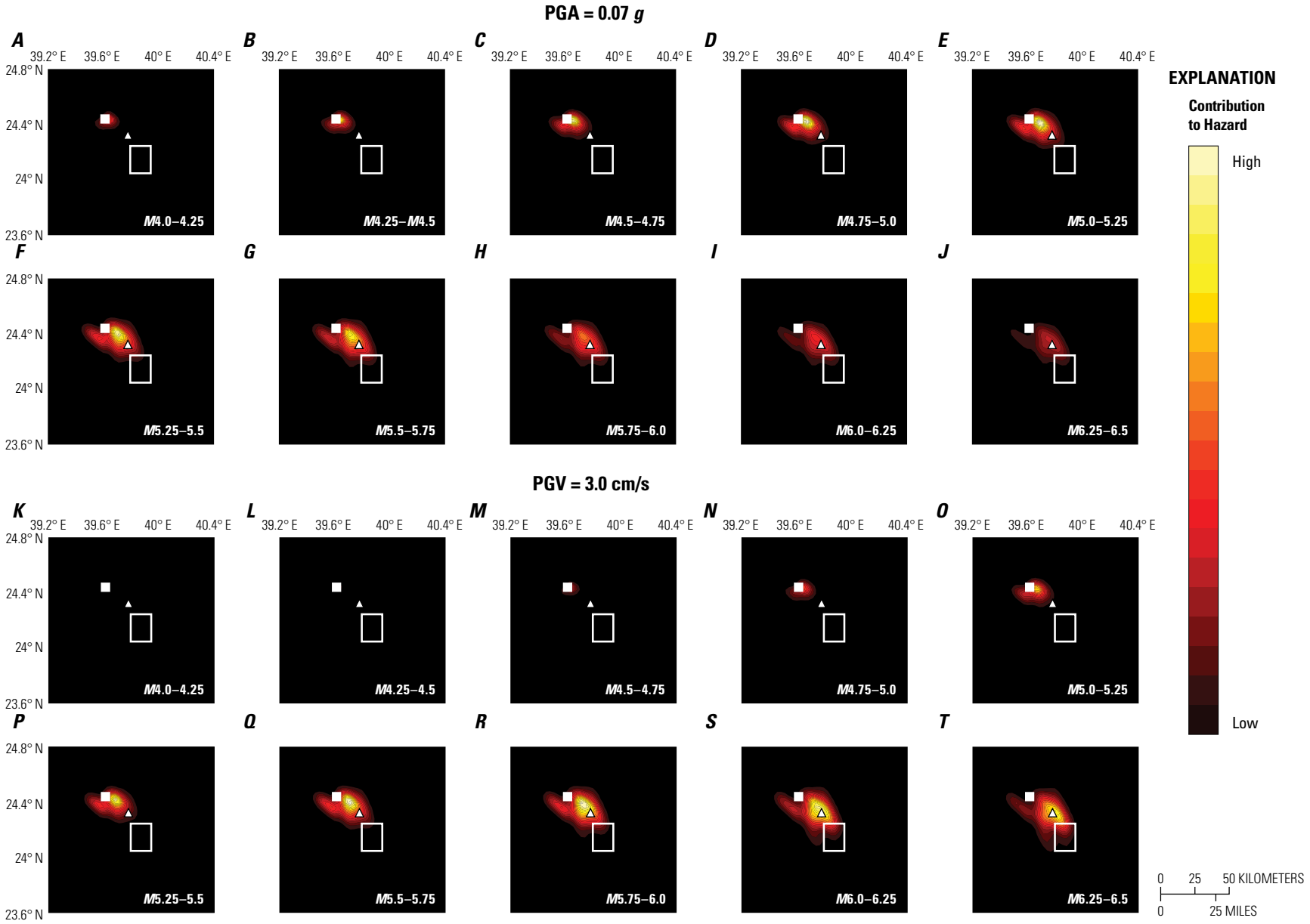

Figure 7. Maps showing deaggregation results for source locations affecting the center of Al Madīnah for both peak ground acceleration (PGA) (*A*–*J*) and peak ground velocity (PGV) (*K*–*T*). Deaggregation yields a PGA value of 0.07 standard gravity (*g*) and a PGV value of 3 centimeters per second (cm/s). These values are estimated as a 2-percent probability of exceedance in 50 years (2,475-year return period) using the spatial distribution of Dietterich and others (2017) displayed in figure 3*B*. White square shows center of Al Madīnah, white triangle shows vent location of the 1256 C.E. eruption, and white outlined rectangle shows location of the 1999 seismic swarm.

center; and (3) the youngest eruption sites were concentrated between lat 24.2° N. and 24.35° N. and show no discernable temporal propagation toward the city center.

Discussion

The Saudi Arabia seismic-hazard maps published by Zahran and others (2015, 2016) and Sokolov and others (2017) do not include possible earthquakes occurring in northern Harrat Rahat. The predicted PGA level for a 2-percent probability of exceedance in 50 years in northern Harrat Rahat is nearly uniform at 0.08 *g* in the map of Zahran and others (2015) and less than 0.05 *g* in the map of Sokolov and others (2017). The level of ground motion predicted by Zahran and others (2015) in northern Harrat Rahat is similar to our results near Al Madīnah. The main contribution to a PGA value of 0.08 *g* in northern Harrat Rahat predicted by Zahran and others (2015) is a potential large earthquake in Harrat Lunayyir, which is about 200 km from Al Madīnah. However, an updated analysis (Zahran and El-Hady, 2017) indicates that the source area in Harrat Lunayyir was overestimated, so the PGA calculated for Al Madīnah and its vicinity are less than their previous value of 0.08 *g*. In the PSHA published by Sokolov and others (2017), seismicity related to volcanic activity in Harrat Rahat was not considered. Our new results estimating a higher level of ground motion in the area near Al Madīnah is a consequence of considering nearby volcano-related earthquake sources in northern Harrat Rahat.

We also performed PSHA using circular, uniformly distributed spatial probabilities of volcanic eruptions in addition to the probability based on the volcanic vents described by Dietterich and others (2017). This calculation was done to account for the possibility of a large earthquake anywhere in the region. Our motivation was the observation that an earthquake associated with volcanic activity may occur quite far from the vent. Most importantly, there is concern that an earthquake might occur very close to Al Madīnah. The center of the circularly uniform distribution is assumed to be the location of the most probable vent opening (Dietterich and others, 2017) and a 30-km radius is adopted based on the size of the volcanic field. The calculated ground motion levels of PGA and PGV in the case of a 2-percent probability of exceedance in 50 years are about 0.1 *g* and 8 cm/s, respectively, at the most probable vent opening location and 0.06 *g* and 5 cm/s, respectively, at the center of Al Madīnah (fig. 4). The distributions of expected ground motion levels for both PGA and PGV show smaller peak values but spatially extended larger values. Compared to using the volcanic vent model of Dietterich and others (2017) for the spatial distribution, the assumed circularly uniform distributed probabilities do not concentrate in a small area and extend to a wider area, which accounts for the pattern of expected ground motion. The consideration of this example that includes a large earthquake close to Al Madīnah yields a value of probabilistic ground-motion level in the city interior that is about the same as using the volcanic vent model of Dietterich and others (2017).

There is a low probability of a large earthquake happening close to Al Madīnah; therefore, we suggest that the deterministic seismic hazard can be estimated by calculating the ground motion for a scenario earthquake. This relates to the difference between the information provided by probabilistic seismic-hazard estimation and calculations based on deterministic scenarios for low-probability worst-case earthquakes.

The 2007 Saudi Building Code (Saudi Building Code National Committee, 2007) provides regulations and control on the design, construction, quality of materials, and minimum engineering standards. The requirements and recommendations in these building codes provide guidance to ensure that all structures are designed and constructed to resist the effects of strong earthquake ground motions. However, many older buildings in Al Madīnah are reinforced concrete structures built before the effects of seismic loads were well understood (Alguhane and others, 2016). We note that in 1982 a *M*6 earthquake in northern Yemen caused 2,800 fatalities and damaged 300 villages (Choy and Kind, 1987). Hence, the retrofitting of old buildings to resist the damage caused by earthquake ground motion is an important issue in Al Madīnah. This PSHA study can contribute to an ongoing reevaluation of Saudi Arabian building codes.

Conclusions

We carried out a probabilistic seismic hazard analysis (PSHA) for northern Harrat Rahat, Kingdom of Saudi Arabia, a major volcanic field in the west-central part of the Arabian Peninsula with young and frequent magmatic activity. We used recently developed ground-motion prediction equations (Kiuchi and others, 2019) and made three key assumptions: (1) the recurrence interval of local magnitude (M_L) 6.25 earthquakes is equivalent to the return period of volcanic eruptions in the area; (2) the earthquake magnitude-frequency relationship (*b*-value) of 0.895 determined by Zahran and El-Hady (2017) for nearby Harrat Lunayyir is appropriate for northern Harrat Rahat; and (3) the spatial distribution of seismicity follows the spatial probability of the next volcanic vent opening. The size of earthquakes considered is between M_L 3 and 6.5, with earthquake frequency-magnitude relations characterized by the Gutenberg-Richter law. The values of peak ground acceleration (PGA) and peak ground velocity (PGV) in the derived seismic-hazard map with a 2-percent probability of exceedance in 50 years are predicted to be 0.16 acceleration due to gravity (*g*) and 7 centimeters per second (cm/s) at the most probable vent opening location (about 25 km south-southeast of the city center) and about 0.07 *g* and 3 cm/s at the center of Al Madīnah, respectively. In comparison with other published PSHA results, the predicted ground-motion levels obtained in this analysis are generally higher than determined by Sokolov and others (2017) and Zahran and El-Hady (2017) because those studies did not consider nearby sources located within the Harrat Rahat volcanic field.

References Cited

Abdelwahed, M.F., El-Masry, N., Moufti, M.R., Kenedi, C.L., Zhao, D., Zahran, H., and Shawali, J., 2016, Imaging of magma intrusions beneath Harrat Al-Madinah in Saudi Arabia: Journal of Asian Earth Sciences, v. 120, p. 17–28, https://doi.org/10.1016/j.jseaes.2016.01.023.

Aizawa, K., Kanda, W., Ogawa, Y., Iguchi, M., Yokoo, A., Yakiwara, H., and Sugano, T., 2011, Temporal changes in electrical resistivity at Sakurajima volcano from continuous magnetotelluric observations: Journal of Volcanology and Geothermal Research, v. 199, no. 1-2, p. 165–175, https://doi.org/10.1016/j.jvolgeores.2010.11.003.

Alguhane, T.M., Khalil, A., Fayed, M., and Ismail, A., 2016, Pushover analysis of reinforced concrete buildings using full jacket technics—A case study on an existing old building in Madinah: International Journal of Architectural, Civil and Construction Sciences, v. 10, no. 12, p. 1670–1679.

Ambraseys, N.N., Melville, C.P., and Adams, R.D., 2005, The seismicity of Egypt, Arabia, and the Red Sea—A historical review: Cambridge, United Kingdom, Cambridge University Press, 181 p.

Baer, G., and Hamiel, Y., 2010, Form and growth of an embryonic continental rift—InSAR observations and modelling of the 2009 western Arabia rifting episode: Geophysical Journal International, v. 182, p. 155–167, https://doi.org/10.1111/j.1365-246x.2010.04627.

Baker, J.W., Bradley, B.A., Stafford, P.J., 2021, Seismic hazard and risk analysis: Cambridge, United Kingdom, Cambridge University Press, 582 p.

Bedrosian, P.A., Peacock, J.R., Dhary, M., Sharif, A., Feucht, D.W., and Zahran, H., 2019, Crustal magmatism and anisotropy beneath the Arabian shield—A cautionary tale: Journal of Geophysical Research, v. 124, no. B10, p. 10153–10179, https://doi.org/10.1029/2019JB017903.

Boore, D.M., Stewart, J.P., Seyhan, E., and Atkinson, G.M., 2014, NGA-West2 equations for predicting PGA, PGV, and 5% damped PSA for shallow crustal earthquakes: Earthquake Spectra, v. 30, no. 3, p. 1057–1085, https://doi.org/10.1193/070113EQS184M.

Bozorgnia, Y., Abrahamson, N.A., Al Atik, L., Ancheta, T.D., Atkinson, G.M., Baker, J.W., Baltay, A., Boore, D.M., Campbell, K.W., Chiou, B.S.-J., Darragh, R., Day, S., Donahue, J., Graves, R.W., Gregor, N., Hanks, T., Idriss, I.M., Kamai, R., Kishida, T., Kottke, A., Mahin, S.A., Rezaeian, S., Rowshandel, B., Seyhan, E., Shahi, S., Shantz, T., Silva, W., Spudich, P., Stewart, J.P., Watson-Lamprey, J., Wooddell, K., and Youngs, R., 2014, NGA-West2 Research Project: Earthquake Spectra, v. 30, no. 3, p. 973–987, https://doi.org/10.1193/072113EQS209M.

Brown, G.F., Schmidt, D.L., and Huffman, A.C., Jr., 1989, Geology of the Arabian Peninsula—Shield area of western Saudi Arabia: U.S. Geological Survey Professional Paper 560–A, 188 p., https://doi.org/10.3133/pp560A.

Camp, V.E., Hooper, P.R., Roobol, J.M., and White, D.L., 1987, The Madinah eruption, Saudi Arabia—Magma mixing and simultaneous extrusion of three basaltic chemical types: Bulletin of Volcanology, v. 49, no. 2, p. 489–508.

Camp, V.E., and Roobol, M.J., 1989, The Arabian continental alkali basalt province—Part I. Evolution of Harrat Rahat, Kingdom of Saudi Arabia: Geological Society of America Bulletin, v. 101, no. 1, p. 71–95.

Camp, V.E., and Roobol, M.J., 1991, Geologic map of the Cenozoic lava field of Harrat Rahat, Kingdom of Saudi Arabia: Saudi Arabian Deputy Ministry for Mineral Resources Geoscience Map GM–123, scale 1:250,000, 37 p.

Chang, S.-J., Merino, M., Van der Lee, S., Stein, S., and Stein, C.A., 2011, Mantle flow beneath Arabia offset from opening of the Red Sea: Geophysical Research Letters, v. 38, no. 4, 5 p., https://doi.org/10.1029/2010GL045852.

Choy, G.L., and Kind, R., 1987, Rupture complexity of a moderate-sized (mb 6.0) earthquake—Broadband body-wave analysis of the North Yemen earthquake of 13 December 1982: Bulletin of the Seismological Society of America, v. 77, no. 1, p. 28–46.

Civilini, F., Mooney, W.D., Savage, M.K., Townend, J., and Zahran, H., 2019, Crustal imaging of northern Harrat Rahat, Saudi Arabia, from ambient noise tomography: Geophysical Journal International, v. 219, no. 3, p. 1532–1549, https://doi.org/10.1093/gji/ggz380.

Coleman, R.G., Gregory, R.T., and Brown, G.F., 1983, Cenozoic volcanic rocks of Saudi Arabia: U.S. Geological Survey Open-File Report 83–788, 82 p.

Dietterich, H.R., Downs, D.T., and Stelten, M.E., 2023, Lava flow emplacement in Harrat Rahat with implications for eruptions in mafic volcanic fields, chap. E *of* Sisson, T.W., Calvert, A.T., and Mooney, W.D., eds., Active volcanism on the Arabian Shield—Geology, volcanology, and geophysics of northern Harrat Rahat and vicinity, Kingdom of Saudi Arabia: U.S. Geological Survey Professional Paper 1862 [also released as Saudi Geological Survey Special Report SGS–SP–2021–1], 49 p., https://doi.org/10.3133/pp1862E.

Dietterich, H.R., Downs, D.T., Stelten, M.E., and Zahran, H., 2018, Reconstructing lava flow emplacement histories with rheological and morphological analyses—The Harrat Rahat volcanic field, Kingdom of Saudi Arabia: Bulletin of Volcanology, v. 80, no. 12, 23 p., https://doi.org/10.1007/s00445-018-1259-4.

Dietterich, H.R., Stelten, M.E., Downs, D.T., and Champion, D.E., 2017, Spatial and temporal analysis of eruption locations, compositions, and styles in Northern Harrat Rahat, Kingdom of Saudi Arabia [abs.]: Eos, Transactions, American Geophysical Union, Fall Meeting Supplement, no. V51B-1333.

Downs, D.T., Robinson, J.E., Stelten, M.E., Champion, D.E., Dietterich, H.R., Sisson, T.W., Zahran, H., Hassan, K., and Shawali, J., 2019, Geologic map of the northern Harrat Rahat volcanic field, Kingdom of Saudi Arabia: U.S. Geological Survey Scientific Investigations Map 3428 [also released as Saudi Geological Survey Special Report SGS–SP–2019–2], 65 p., 4 sheets, scales 1:75,000, 1:25,000, https://doi.org/10.3133/sim3428.

Downs, D.T., Stelten, M.E., Champion, D.E., Dietterich, H.R., Nawab, Z., Zahran, H., Hassan, K., and Shawali, J., 2018, Volcanic history of the northernmost part of the Harrat Rahat volcanic field, Saudi Arabia: Geosphere, v. 14, no. 3, p. 1253–1282, https://doi.org/10.1130/GES01625.1.

Downs, D.T., Stelten, M.E., Dietterich, H.R., Champion, D.E., Mahood, G.A., Sisson, T.W., Calvert, A.T., and Shawali, J., 2023, Explosive trachyte eruptions from the Al Efairia volcanic center in northern Harrat Rahat, Kingdom of Saudi Arabia, chap. G *of* Sisson, T.W., Calvert, A.T., and Mooney, W.D., eds., Active volcanism on the Arabian Shield—Geology, volcanology, and geophysics of northern Harrat Rahat and vicinity, Kingdom of Saudi Arabia: U.S. Geological Survey Professional Paper 1862 [also released as Saudi Geological Survey Special Report SGS–SP–2021–1], 14 p., https://doi.org/10.3133/pp1862G.

Eissler, H.K., and Kanamori, H., 1987, A single-force model for the 1975 Kalapana, Hawaii, earthquake: Journal of Geophysical Research, v. 92, no. B6, p. 4827–4836, https://doi.org/10.1029/JB092iB06p04827.

El Difrawy, M.A., Runge, M.G., Moufti, M.R., Cronin, S.J., and Bebbington, M., 2013, A first hazard analysis of the Quaternary Harrat Al Madīnah volcanic field, Saudi Arabia: Journal of Volcanology and Geothermal Research, v. 267, p. 39–46, https://doi.org/10.1016/j.jvolgeores.2013.09.006.

Gutenberg, B., and Richter, C.F., 1944, Frequency of earthquakes in California: Bulletin of the Seismological Society of America, v. 34, no. 4, p. 185–188.

Kaban, M.K., El Khrepy, S., Al-Arifi, N., Tesauro, M., and Stolk, W., 2016, Three-dimensional density model of the upper mantle in the Middle East—Interaction of diverse tectonic processes: Journal of Geophysical Research, v. 212, no. B7, p. 5349–5364, https://doi.org/10.1002/2015JB012755.

Kehoe, H.L., Kiser, E.D., and Okubo, P.G., 2019, The rupture process of the 2018 M w 6.9 Hawai‘i earthquake as imaged by a genetic algorithm-based back-projection technique: Geophysical Research Letters, v. 46, no. 5, p. 2467–2474, https://doi.org/10.1029/2018GL080397.

Kiuchi, R., Mooney, W.D., and Zahran, H.M., 2019, Ground-motion prediction equations for western Saudi Arabia: Bulletin of the Seismological Society of America, v. 109, no. 6, p. 2722–2737, https://doi.org/10.1785/0120180302.

Klein, F.W., and Wright, T., 2008, Exponential decline of aftershocks of the M7.9 1868 great Kau earthquake, Hawaii, through the 20th century: Journal of Geophysical Research, v. 113, no. B9, 11 p, https://doi.org/10.1029/2007JB005411.

Langenheim, V.E., Ritzinger, B.T., Zahran, H., Shareef, A., and Al-dahri, M., 2019, Crustal structure of the northern Harrat Rahat volcanic field (Saudi Arabia) from gravity and aeromagnetic data: Tectonophysics, v. 750, p. 9–21, https://doi.org/10.1016/j.tecto.2018.11.005.

Langenheim, V.E., Ritzinger, B.T., Zahran, H.M., Shareef, A., and Al-Dhahry, M.K., 2023, Depth to basement and crustal structure of the northern Harrat Rahat volcanic field, Kingdom of Saudi Arabia, from gravity and aeromagnetic data, chap. K *of* Sisson, T.W., Calvert, A.T., and Mooney, W.D., eds., Active volcanism on the Arabian Shield—Geology, volcanology, and geophysics of northern Harrat Rahat and vicinity, Kingdom of Saudi Arabia: U.S. Geological Survey Professional Paper 1862 [also released as Saudi Geological Survey Special Report SGS–SP–2021–1], 18 p., https://doi.org/10.3133/pp1862K.

Lindsay, J.M., and Moufti, M.R., 2014, Assessing volcanic risk in Saudi Arabia: Eos Transactions, v. 95, no. 31, p. 277–278, https://doi.org/10.1002/2014EO310002.

Lipman, P.W., and Calvert, A.T., 2013, Modeling volcano growth on the Island of Hawaii—Deep-water perspectives: Geosphere, v. 9, no. 5, p. 1348–1383, https://doi.org/10.1130/GES00935.1.

Llenos, A.L., and Michael, A.J., 2022, Modeling the occurrence of M ~5 caldera collapse-related earthquakes in Kīlauea Volcano, Hawai‘i: Geophysical Research Letters, v. 49, no. 1, 9 p., https://doi.org/10.1029/2020GL092242.

Marzocchi, W., and Taroni, M., 2014, Some thoughts on declustering in probabilistic seismic-hazard analysis: Bulletin of the Seismological Society of America, v. 104, no. 4, p. 1838–1845, https://doi.org/10.1785/0120130300.

McGuire, R.K., 2008, Probabilistic seismic hazard analysis—Early history: Earthquake Engineering & Structural Dynamics, v. 37, no. 3, p. 329–338, https://doi.org/10.1002/eqe.765.

Moufti, M.R., and Németh, K., 2016, Geoheritage of volcanic harrats in Saudi Arabia: Switzerland, Springer, 194 p.

Murcia, H., Németh, K., Moufti, M.R., Lindsay, J.M., El-Masry, N., Cronin, S.J., Qaddah, A., and Smith, I.E.M., 2014, Late Holocene lava flow morphotypes of northern Harrat Rahat, Kingdom of Saudi Arabia—Implications for the description of continental lava fields: Journal of Asian Earth Sciences, v. 84, p. 131–145, https://doi.org/10.1016/j.jseaes.2013.10.002.

Pallister, J.S., McCausland, W.A., Jónsson, S., Lu, Z., Zahran, H.M., El Hadidy, S., Aburukbah, A., Stewart, I.C.F., Lundgren, P.R., White, R.A., and Moufti, M.R.H., 2010, Broad accommodation of rift-related extension recorded by dyke intrusion in Saudi Arabia: Nature Geoscience, v. 3, no. 10, p. 705–712, https://doi.org/10.1038/ngeo966.

Peacock, J.R., Bedrosian, P.A., Al-Dhahry, M.K., Shareef, A., Feucht, D.W., Taylor, C.D., Bloss, B., and Zahran, H.M., 2023, Magnetotelluric investigation of northern Harrat Rahat, Kingdom of Saudi Arabia, chap. L *of* Sisson, T.W., Calvert, A.T., and Mooney, W.D., eds., Active volcanism on the Arabian Shield—Geology, volcanology, and geophysics of northern Harrat Rahat and vicinity, Kingdom of Saudi Arabia: U.S. Geological Survey Professional Paper 1862 [also released as Saudi Geological Survey Special Report SGS–SP–2021–1], 111 p., https://doi.org/10.3133/pp1862L.

Petersen, M.D., Moschetti, M.P., Powers, P.M., Mueller, C.S., Haller, K.M., Frankel, A.D., Zeng, Y., Rezaeian, S., Harmsen, S.C., Boyd, O.S., Field, N., Chen, R., Rukstales, K.S., Luco, N., Wheeler, R.L., Williams, R.A., and Olsen, A.H., 2015, The 2014 United States National Seismic Hazard Model: Earthquake Spectra, v. 31, S1, p. S1–S30, https://doi.org/10.1193/120814EQS210M.

Reilinger, R., and McClusky, S., 2011, Nubia-Arabia-Eurasia plate motions and the dynamics of Mediterranean and Middle East tectonics: Geophysical Journal International, v. 186, no. 3, p. 971–979, https://doi.org/10.1111/j.1365-246X.2011.05133.x.

Saudi Building Code National Committee, 2007, Saudi Building Code SBC-301-2007, loads and forces requirements: Riyadh, Kingdom of Saudi Arabia, Saudi Building Code National Committee, 67 p.

Sokolov, V., Zahran, H.M., Youssef, S.E.H., El-Hadidy, M., and Alraddadi, W.W., 2017, Probabilistic seismic hazard assessment for Saudi Arabia using spatially smoothed seismicity and analysis of hazard uncertainty: Bulletin of Earthquake Engineering, v. 15, no. 7, p. 2695–2735, https://doi.org/10.1007/s10518-016-0075-5.

Stelten, M.E., Downs, D.T., Champion, D.E., Dietterich, H.R., Calvert, A.T., Sisson, T.W., Mahood, G.A., and Zahran, H., 2020, The timing and compositional evolution of volcanism within northern Harrat Rahat, Kingdom of Saudi Arabia: Geological Society of America Bulletin, v. 132, no. 7–8, p. 1381–1403.

Stelten, M.E., Downs, D.T., Champion, D.E., Dietterich, H.R., Calvert, A.T., Sisson, T.W., Mahood, G.A., and Zahran, H.M., 2023, Eruptive history of northern Harrat Rahat—Volume, timing, and composition of volcanism over the past 1.2 million years, chap. D *of* Sisson, T.W., Calvert, A.T., and Mooney, W.D., eds., Active volcanism on the Arabian Shield—Geology, volcanology, and geophysics of northern Harrat Rahat and vicinity, Kingdom of Saudi Arabia: U.S. Geological Survey Professional Paper 1862 [also released as Saudi Geological Survey Special Report SGS–SP–2021–1], 46 p., https://doi.org/10.3133/pp1862D.

Stelten, M.E., Downs, D.T., Dietterich, H.R., Mahood, G.A., Calvert, A.T., Sisson, T.W., Zahran, H., and Shawali, J., 2018, Timescales of magmatic differentiation from alkali basalt to trachyte within the Harrat Rahat volcanic field, Kingdom of Saudi Arabia: Contributions to Mineralogy and Petrology, v. 173, 17 p., https://doi.org/10.1007/s00410-018-1495-9.

Yao, Z.X., Mooney, W.D., Zahran, H.M., and Youssef, S.E.-H., 2017, Upper mantle velocity structure from Rayleigh surface wave tomography and its implications: Journal of Geophysical Research, v. 122, no. B8, p. 6552–6568, https://doi.org/10.1002/2016JB013805.

Yokoyama, I., 1986, Crustal deformation caused by the 1914 eruption of Sakurajima volcano, Japan and its secular changes: Journal of Volcanology and Geothermal Research, v. 30, no. 3-4, p. 283–304.

Zahran, H.M., and El-Hady, S.M., 2017, Seismic hazard assessment for Harrat Lunayyir—A lava field in western Saudi Arabia: Soil Dynamics and Earthquake Engineering, v. 100, p. 428–444, https://doi.org/10.1016/j.soildyn.2017.06.009.

Zahran, H.M., Sokolov, V., El-Hadidy, S.Y., and Alraddi, W.W., 2015, Preliminary probabilistic seismic hazard assessment for the Kingdom of Saudi Arabia based on combined areal source model—Monte Carlo approach and sensitivity analyses: Soil Dynamics and Earthquake Engineering, v. 77, p. 453–468, https://doi.org/10.1016/j.soildyn.2015.06.011.

Zahran, H.M., Sokolov, V., Roobol, M.J., Stewart, I.C.F., El-Hadidy Youssef, S., and El-Hadidy, S., 2016, On the development of a seismic source zonation model for seismic hazard assessment in western Saudi Arabia: Journal of Seismology, v. 20, no. 3, p. 747–769, https://doi.org/10.1007/s10950-016-9555-y.

Moffett Field Publishing Service Center, California
Manuscript approved June 30, 2022
Edited by Regan Austin
Layout and design by Kimber Petersen
Illustration support by Katie Sullivan

Kiuchi and others—**Ground-Motion Prediction Equations for the Western Kingdom of Saudi Arabia**—Professional Paper 1862–O

ISSN 1044-9612 (print)
ISSN 2330-7102 (online)
https://doi.org/10.3133/pp1862O